Earth and Planetary Science Letters 367 (2013) 52–60

Contents lists available at SciVerse ScienceDirect

Earth and Planetary Science Letters

journal homepage: www.elsevier.com/locate/epsl

# Slow slip event in the Mexican subduction zone: Evidence of shallower slip in the Guerrero seismic gap for the 2006 event revealed by the joint inversion of InSAR and GPS data

O. Cavalié [a,b,*], E. Pathier [a], M. Radiguet [a,c], M. Vergnolle [a,b], N. Cotte [a], A. Walpersdorf [a], V. Kostoglodov [d], F. Cotton [a]

[a] Institut des Sciences de la Terre, Université de Grenoble 1, CNRS UMR 5265, F-38041 Grenoble, France
[b] Géoazur, Université de Nice Sophia-Antipolis, CNRS, IRD, Observatoire de la Côte d'Azur, 250 avenue Einstein, 06560 Valbonne, France
[c] Computational Solid Mechanics Laboratory, Ecole Polytechnique Fédérale de Lausanne, EPFL ENAC IIC LSMS, GC A2, Station 18, 1015 Lausanne, Switzerland
[d] Instituto de Geofísica, Universidad Nacional Autónoma de México, Mexico

A R T I C L E I N F O

*Article history:*
Received 19 June 2012
Received in revised form
16 February 2013
Accepted 17 February 2013
Editor: P. Shearer

*Keywords:*
InSAR
slow slip event
subduction zone processes
seismic cycle

A B S T R A C T

Slow slip events (SSEs) in subduction zones have been observed in the last decade with continuous GPS stations. Some of them could be related to the lateral segmentation of subduction interface that seems to be a critical parameter for the propagation of large subduction earthquakes. In 2006, one of the largest SSEs recorded so far was captured by a dozen continuous GPS stations, in the Guerrero area (Mexico) along the Mexican subduction zone. Previous studies based on these data suggested a lateral variation of the updip depth of the SEE at the Guerrero seismic gap, but suffered from a lack of resolution east of the gap. Here, we show the ability of InSAR technique to capture a part of the 2006 SSE cumulative displacement east of the Guerrero gap by a stacking approach. We processed long strip Envisat interferograms corrected for orbital errors and interseismic signal using GPS data. We first use a forward modelling approach to test InSAR sensitivity to the amount of slip, depth and width of the slipping area on the subduction interface. Due to its high spatial resolution, InSAR allows one to comprehensively sample the North–South spatial wavelength of the SSE deformation, complementing the sparse GPS network. InSAR locates the maximum of uplift and subsidence caused by the SSE more precisely than the GPS data, giving better constraints on the updip slip limit of the SSE. We then inverted the InSAR and GPS data separately to understand how each inversion resolves the slip at depth. Finally, we performed a joint inversion of InSAR and GPS data, which constrained the SSE slip and its location on the plate interface over the entire Guerrero area. The joint inversion shows significant lateral variation of the SSE slip distribution along the trench with a shallower updip edge in the Guerrero seismic gap, west of Acapulco, and a deeper slip edge further east.



## 1. Introduction

Precise geodetic measurements, essentially GPS, allowed the discovery of slow transient dislocations in subduction zones such as slow slip events (SSEs) in Japan (e.g., Hirose and Obara, 2005), Cascadia (e.g., Dragert et al., 2004) and Mexico (e.g., Kostoglodov et al., 2003). The increasing number of observations in different regions has shown a variability in the duration, magnitude and recurrence of slow slip events (Ide et al., 2007). Moreover, some subduction areas present a clear correlation in time and space between non-volcanic tremor (NVT) and SSE, for example in Cascadia. Contrastingly in Mexico, these two phenomena are not directly associated: most of the NVT episodes occur downdip of the long-term SSE area and there is high NVT activity which is not correlated in time with large slow slip events (Payero et al., 2008; Kostoglodov et al., 2010). Precise determination of the slip distribution at depth and along the subduction trench is essential to reveal the physical processes involved in the slow slip events, and to understand their role in the seismic cycle of large subduction earthquakes. This study focuses on the Guerrero segment of the subduction zone in Mexico, where one of the best-recorded series of SSEs in the world exists. In this region, the subduction interface between the Cocos and North America plates is relatively flat, becoming steeper on both sides of this area

* Corresponding author at: Géoazur, Université de Nice Sophia-Antipolis, CNRS, IRD, Observatoire de la Côte d'Azur, 250 avenue Einstein, 06560 Valbonne, France. Tel.: +33 4 92 94 26 74.
*E-mail addresses:* ocavalie@geoazur.unice.fr (O. Cavalié), erwan.pathier@ujf-grenoble.fr (E. Pathier).

0012-821X/$ - see front matter © 2013 Elsevier B.V. All rights reserved.
http://dx.doi.org/10.1016/j.epsl.2013.02.020

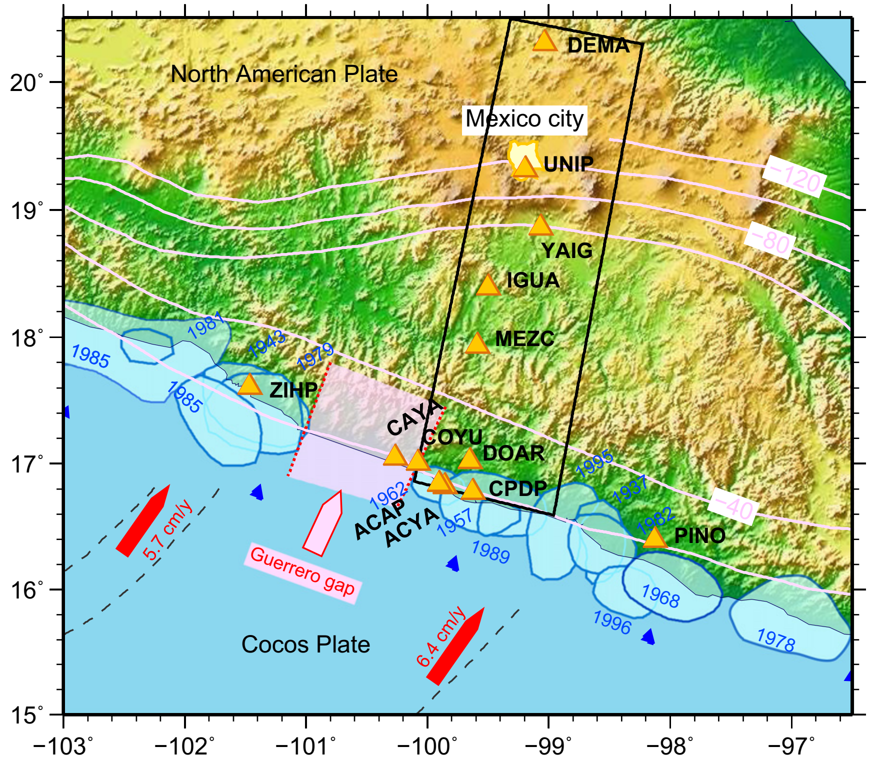


**Fig. 1.** Tectonic map of the Cocos-North America (NA) plates convergence zone in Central Mexico (from Kostoglodov et al., 2003). The dashed blue line represents the Middle America trench and the magnitude of the red arrows indicate the Cocos-NA convergence velocities (Demets et al., 2010). Pink lines denote the depth of the interface between the Cocos and NA plates. Blue patches represent the major earthquakes rupture zones. The locations of permanent GPS stations are indicated by orange triangles. The black rectangle indicates the coverage of the Envisat radar images used in this study (track 255, I2, stripmap mode). (For interpretation of the references to color in this figure legend, the reader is referred to the web version of this article.)

(Fig. 1). The largest crustal displacements during the SSEs have been observed in the Guerrero seismic gap area,[1] a $\sim 120$ km-long segment of the seismogenic zone where no major earthquake has occurred since the $M_s$ 7.6 earthquake in 1911 (e.g., Nishenko and Singh, 1987; Kostoglodov and Ponce, 1994). If the recurrence period of large historical subduction thrust earthquakes in Mexico is of 30–60 yrs, then an earthquake in the Guerrero gap is overdue already. This raises the question of a possible relationship between the existence of a persisting seismic gap and the occurrence of large SSEs (Lowry et al., 2001; Kostoglodov et al., 2003; Yoshioka et al., 2004; Larson et al., 2007).

A related question is whether the SSEs are intruding into the seismogenic zone (e.g., Larson et al., 2004). This information is crucial to know how the subduction margin is segmented. A recurrent aseismic slip located in the seismogenic layer in the Guerrero seismic gap could act as a barrier and thus control the spatial extension of a potential mega-earthquake in the area. On the other hand, a deeper SSE location could increase the stress in the seismogenic zone and thus increase the probability of a mega-thrust event (Mazzotti and Adams, 2004). The 2011 Tohoku-Oki earthquake showed that understanding the lateral segmentation of a subduction zone has a huge impact on seismic hazard evaluation. Before the earthquake, Japanese hazard maps divided the offshore subduction interface located north of Tokyo into six segments, each roughly 150 km long (Kerr, 2011). This distribution, based on the past known seismicity, restricted drastically the probability of a mega-earthquake occurrence along this stretch of the Japan trench. However, based on GPS data, Loveless and Meade (2010) showed that the interseismic coupling did not respect this segmentation, and actually the Tohoku-Oki mega-earthquake broke the plane along a much bigger area than predicted by the hazard map. Knowing in details the lateral variations of the subduction dynamic along the trench is then a key point to properly assess its seismic hazard. The Mexican GPS network recorded the first large slow slip event in 1998 and since then SSEs occur on a cycle of about 4 yrs. However, individual events have different spatial and temporal characteristics (Radiguet et al., 2012). For instance, their durations range from 6 to 14 months; the longest duration was recorded for the SSE from July 2009 to September 2010 (Walpersdorf et al., 2011). The estimated values of fault slip are among the largest reported worldwide for periodic SSE (e.g., Ide et al., 2007), generating surface displacements up to 6 cm. The 2006 event occurred between April 2006 and February 2007 (Vergnolle et al., 2010) with an equivalent seismic moment estimated at $2.2 \times 10^{20}$ Nm (Larson et al., 2007), corresponding to an equivalent $M_W$ 7.5 earthquake. The GPS network designed to monitor the long-term interseismic deformation and SSE consists primarily of a North–South trench-perpendicular profile from the coast up to Mexico City, and a trench-parallel profile running along the coast. Despite efforts to increase the GPS network coverage since the discovery of the Guerrero SSEs in 1998 (Lowry et al., 2001), the spatial extent of the surface deformation remains poorly constrained, especially considering its inland East–West variation. For instance, the spatial extent of the 2006 SSE was monitored by only a dozen irregularly distributed permanent GPS stations (see Fig. 1). GPS data have been inverted to derive slip distribution on the subduction interface (Larson et al., 2007; Radiguet et al., 2011, 2012). Based on these results, Radiguet et al. (2012) have suggested lateral variations of SSE properties in the Guerrero seismic gap. However, their results suffer from a lack of resolution east of the

[1] Note that the Guerrero Gap is sometimes defined as extending up to longitude 99°W, but in this case two segments are distinguished: the NW Guerrero Gap (called Guerrero Gap in this paper) and the SE Guerrero Gap on which several earthquakes have occurred since 1911, e.g., 1957, 1962, 1989, 1995 (see Fig. 1, Suárez et al., 1990; Ortiz et al., 2000).

gap. Indeed, the reliability of the inverted distribution away from the two main GPS profiles remains an issue. And even along the profiles, the GPS network is not dense enough to properly sample the SSE crustal deformation. The lack of resolution of the past results only based on GPS data is a strong motivation for using space-borne Synthetic Aperture Radar Interferometry technique (InSAR). Due to its high spatial sampling, InSAR (e.g., Bürgmann et al., 2000) has the potential to provide far denser measurements of the surface displacement than sparse GPS network. In spite of vegetation cover and mountainous zones in the Guerrero area, which are usually limiting factors of C-band InSAR, preliminary results from Cavalié et al. (2009) showed, for the first time, that InSAR was able to capture the 2006 SSE surface displacement. Following this approach, our study uses InSAR to obtain dense surface displacement measurements with an extended coverage (Fig. 1), focusing on the 2006 SSE. The aim of this study is first to test the ability of InSAR to get new constraints for retrieving the SSE characteristics at depth. We then combine GPS and InSAR data sets to provide a better slip distribution model for the 2006 SSE. A further goal is to establish spatial relationships between the SSE and the Guerrero seismic gap.

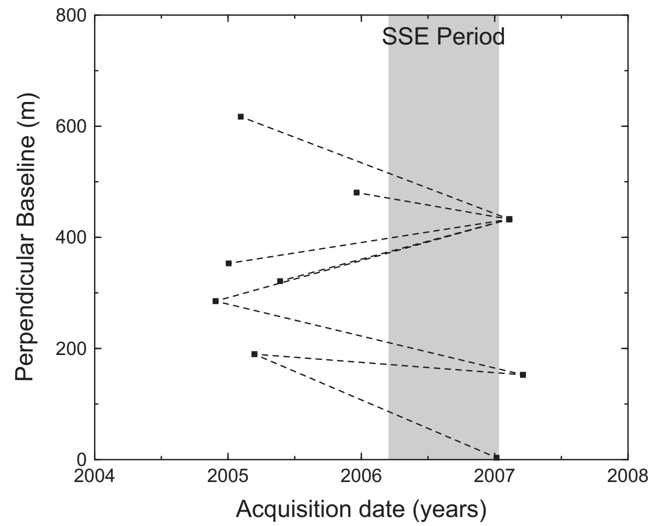


**Fig. 2.** Relative position of Envisat orbits on descending track 255 plotted as a function of image acquisition dates. Dashed lines show the eight interferograms selected for stacking. The gray area indicates the time span of the 2006 slow slip event.

## 2. Data and processing

The present study focuses on the 2006 event because a larger amount of suitable GPS and SAR data is available compared with the previously recorded events. Indeed, the 1998 event was not well documented by GPS (continuous record at only one station (Lowry et al., 2001) and the 2002 event was not well documented by SAR data (ERS-2 satellite had gyroscope problems at this time). InSAR analysis of the last SSE (2009–2010) is in progress but requires another processing strategy because of a different temporal distribution of SAR data. To map the surface displacement associated with the 2006 event, we use data from the Envisat SAR archive provided by the European Space Agency (ESA). Unfortunately, only data on descending tracks are exploitable, impeding the use of ascending data to constrain the SSW horizontal displacement. Among the possible descending tracks covering the Guerrero area, we focus on track 255, which provides the largest number of suitable images for our analysis. Track 255 also covers most of the permanent GPS stations, which are useful for correcting interferograms for orbital uncertainties and for validating InSAR measurements of ground deformation. Along the adjacent track (T26) less suitable images are available, and none of the five processed interferograms were coherent enough to be unwrapped (Chen and Zebker, 2000; Gens, 2003) in the coastal area, where most of the SSE signal is expected. Twelve images (see Table S1), acquired between November 2004 and March 2007 along track 255, were selected according to three criteria: (1) full coverage from the coast to north of Mexico City (around 500 km long) in order to include a far-field area not affected by the SSE, (2) acquisition date close to the SSE to limit temporal decorrelation, and (3) low perpendicular baseline dispersion (Fig. 2) to minimize geometrical decorrelation in interferograms. The ROI-PAC software (Rosen et al., 2004) was used to process the interferograms from raw data. In order to limit the geometrical phase decorrelation, we imposed perpendicular baselines to be smaller than 200 m. As no suitable images were acquired during the SSE with these constraints (Fig. 2), we cannot reconstruct the time evolution of the SSE deformation and therefore the analysis of the SSE finite displacements was only done. Consequently, a stacking approach has been adopted, based on the 12 interferograms that encompass the 2006 SSE. Those interferograms are corrected for orbital and topographic components using DEOS (Scharroo and Visser, 1998) and the 3-arc-second SRTM DEM (Farr and Kobrick, 2000), respectively. The main difficulties encountered during InSAR processing are related to phase decorrelation, which occurs between the coast and Mexico City. This is due to vegetation cover and to the steep slopes in the mountain ranges (Fig. 1). To help the phase unwrapping, interferograms are down-sampled using 32 looks in range and $5 \times 32$ looks in azimuth (Ferretti et al., 2007), resulting in a $\sim 640$ m pixel spacing. The loss of spatial resolution is acceptable, as the expected gradient for the ground displacement due to the SSE is low (a few centimeters distributed over tens of kilometers). This approach has been shown to efficiently recover phase coherence (Jónsson, 2008). Interferograms are then filtered using an adaptive filter (Goldstein and Werner, 1998) for further noise reduction. Some of the 12 interferograms have large areas of low coherence impeding the phase unwrapping. Consequently, eight interferograms (see Fig. 2) with acceptable unwrapped information are used to retrieve the tectonic signal. We correct the long wavelength orbital errors on each interferogram. As the SSE signal affects most of the interferograms, we cannot rely on stable areas to constrain the orbital error. We, thus, use GPS data to adjust a linear ramp in the North–South and East–West direction. A linear rather than a quadratic correction is applied due to the irregular spatial distribution and limited number of GPS stations available (from 5 to 6 depending on the interferogram) impeding a robust estimate of second order polynomial coefficients. The displacement of each GPS station (taken from Vergnolle et al., 2010) occurring between the two acquisition dates is computed along the radar line of sight (LOS). The parameters of the linear ramp are estimated by minimizing the misfit between LOS GPS displacements and InSAR displacements, which are averaged on a $10 \times 10$ pixel window centered on the location of GPS stations. Another correction is needed because the selected interferograms include both SSE deformation and interseismic signals. The amplitude of the latter depends mainly on the acquisition date of the first image (the second images of the interferograms have been acquired very shortly after the end of the SSE). The older the acquisition of the first image, the larger the recorded interseismic signal in the interferogram. Therefore, it is important to calibrate the interferograms containing different amounts of interseismic signal. To quantify the cumulated surface displacement of the SSE, we chose to measure the difference between the station position at a given date after the event (the second date of the SAR image that forms the interferogram) and a theoretical GPS position, based on pre-SSE interseismic displacement rates, supposing that the 2006 event had not occurred. In other words, the cumulated displacement of the SSE corresponds to the deviation from the interseismic trend induced by the SSE. GPS measurements show a relatively constant interseismic velocity between two consecutive SSEs (Vergnolle et al., 2010; Radiguet et al., 2012). Continuous GPS data between 2002 and 2006 have been inverted to compute the inter-SSE coupling on the subducting interface using an inversion scheme similar to Radiguet et al. (2012). We used this model to derive the map of inter-SSE LOS surface displacement rates for each InSAR pixel. This rate is multiplied by the time span of each interferogram and subtracted from the interferogram to get the deviation from the interseismic trend caused by the SSE. After correcting for the interseismic deformation, the interferometric signal consists of the SSE displacement and of remaining perturbations, mainly atmospheric delays. To increase the signal-to-noise ratio and to mitigate the atmospheric perturbation, the eight corrected interferograms (see Fig. S1) are averaged (Zebker et al., 1997; Cavalié et al., 2008).

## 3. InSAR results

Fig. 3 shows the LOS ground displacement due to the 2006 SSE, obtained by averaging the interferogram stack. As the eight interferograms are not unwrapped over the same extent (see Fig. S1), only pixels of the stack where at least five interferograms were available are used (Fig. S2). The cumulated LOS surface displacements of the SSE, as defined in the previous section, range from 5.5 cm (toward the satellite) to −4.8 cm (away from the satellite). It is noteworthy that the LOS displacement is highly correlated to the vertical component because of the small angle ( $\sim 23^{\circ}$) between the LOS and the vertical axis, and because the LOS is nearly orthogonal to the horizontal component of the slow slip event motion. LOS displacement variations are mainly North–South. Thus, the map can be described as showing subsidence south of Mexico City from latitude 18.5°N to 17.6°N, with a maximum of subsidence around 18°N and an uplift from 17.4°N to the coast. The uplift is maximum around 17°N. The standard deviation of the LOS displacement is about 1.3 cm in average but can be up to 3.5 cm, with larger values near the coast where the number of available interferograms is smaller due to unwrapping problem (Figs. S2 and S3). Profiles perpendicular to the trench show no significant deformation north of Mexico City but a long wavelength signal south of it. The maximum LOS displacement is located at about 100–110 km from the trench, and the minimum at about 200–220 km (Fig. 3). Comparison with GPS measurements, projected along LOS, shows a good agreement with a root mean square (RMS) of 0.5 cm (computed at the six stations where InSAR values are available). This RMS is lower than the standard deviation of the LOS displacement. The spatially continuous InSAR measurement confirms that the spatial distribution of the GPS network was not optimal for sampling the displacement signal during the 2006 SSE. Particularly, due to the absence of stations between DOAR and MEZC, the GPS network was not able to determine the uplift peak of the 2006 event. The displacements of the GPS stations close to the coast (ACAP, ACYA, CPDP, and DOAR) are well explained by the decrease in the LOS displacement toward the coastline (Fig. 3). However, the COYU and CAYA stations, which are located about 10 km from the coast but tens of kilometers further west, present LOS displacements significantly higher than ACAP and ACYA, indicating a lateral variation of the surface displacement west of Acapulco (ACAP), an area which is unfortunately not covered by our InSAR measurements. Possible errors due to atmospheric delay have been investigated (Doin et al., 2009). By stacking interferograms, we expect to significantly decrease the random phase delays due to the atmospheric turbulence (Zebker et al., 1997; Hanssen, 2001). This decrease follows a square root function of the number of independent interferograms. On the contrary, the spatially correlated delays (tropostatic delay Cavalié et al., 2007, 2008) do not follow such a relation, and stacking methods are less efficient at removing this effect which is correlated (or anti-correlated) to the elevation. In our results on the 2006 SSE, some local correlations can be found at a kilometric scale (for instance at volcanoes), however, at larger scale there is no significant correlation between elevation and LOS displacements (see profiles

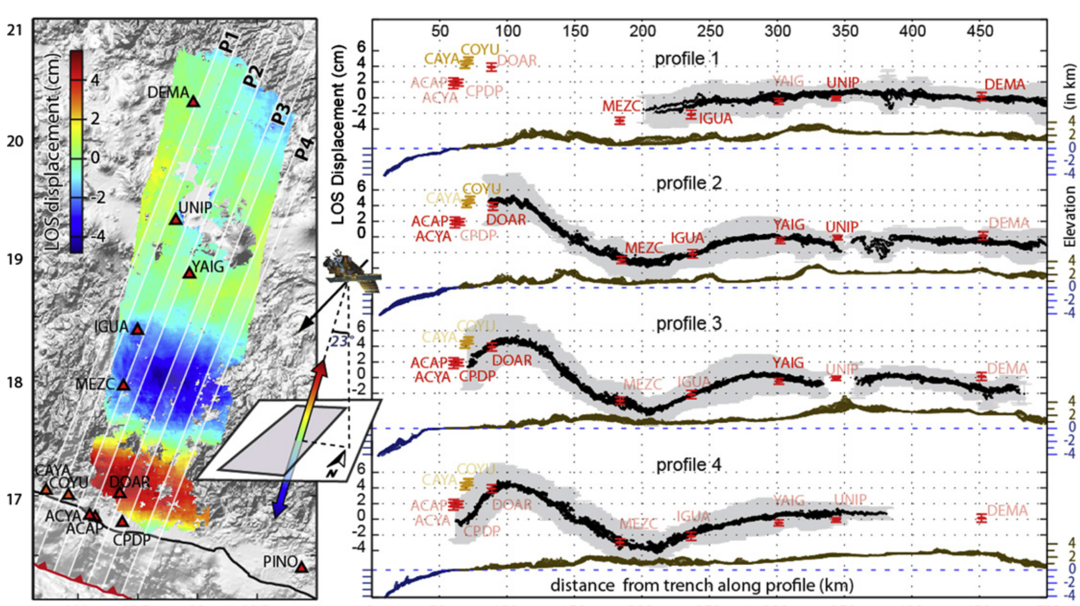


**Fig. 3.** Left panel: Map of surface displacement (in LOS, see drawing) caused by the 2006-SSE. After our processing, only few places stay incoherent: by the coast (north of Acapulco), on the steep slopes of two volcanoes (north-east of YAIG), and in Mexico City (east of UNIP). For this latest area, because of the spatial downsampling, the local high gradient of subsidence in Mexico City (López-Quiroz et al., 2009) causes aliasing, impeding the phase unwrapping. The white boxes (7 km wide) indicate the profile locations shown in the right panel. Right panel: Four profiles, perpendicular to the Middle America trench, showing the LOS displacement estimated from InSAR (black dots, the gray envelope represents the phase standard deviation of the individual interferograms before stacking) and the topography (blue dots offshore and brown dots overland). All InSAR and elevation points located in the white boxes are projected onto the corresponding profile. Red markers show LOS displacements inferred from GPS data. Orange markers are used for the two stations located within the Guerrero gap. Name of GPS stations located more than 10 km away from a profile are shown with a lighter color for this profile. The SSE surface signature is characterized by a smooth deformation with a 6 cm LOS displacement maximum at about 110 km from the trench and a minimum at about 220 km. (For interpretation of the references to color in this figure legend, the reader is referred to the web version of this article.)

in Figs. 3 and S4). Due to the limited number of interferograms used in the stack and its relatively high standard deviation (Figs. S2 and S3), it is possible that residual orbital errors or some effect of atmospheric perturbations not eliminated during the data processing still affect the LOS displacement signal. As we use GPS records to constrain the long wavelength of the signal and then average the interferograms, these errors are likely to propagate into smooth variations of the LOS displacement at a local-scale. The good agreement between InSAR and GPS results also suggests that they are limited to local-scale smooth perturbations of the signal within the error bars. In this case, the spatial position of the maximum and minimum of LOS displacements is a more robust feature than their absolute value. Similarly, the long-wavelength interseismic correction (ranging from −1 cm to 2 cm in LOS), which improves the agreement between InSAR and GPS data (RMS = 5 mm with correction vs. 9 mm without correction), do not significantly change the position of the maximum and minimum of the LOS displacement (Fig. S5). Using an alternative InSAR processing approach (persistent scatterer technique Hooper et al., 2004), Hooper et al. (2012) found a similar position of the maximum and minimum of LOS displacements, as well as a similar range of the SSE displacements.

## 4. Modelling: forward approach

In order to better understand how surface displacement patterns projected along the LOS are controlled by the slip distribution, we performed a forward modelling exploration. This approach aims to see how InSAR is able to give more information about the slip location on the subduction interface. Our direct models are similar to the model of Radiguet et al. (2011), using the same interface geometry and assuming the slip on the interface to be pure thrust. Green's functions are evaluated in a layered elastic half-space using the 1D Earth's crustal model of Hernandez et al. (2001) (Table S2). Assuming a uniform slip distribution, we investigated the influence of three parameters: (1) depth of the updip slip limit from 12 km to 42 km, (2) width of the slipping area from 25 km to 150 km, and (3) slip amount from 6 cm to 20 cm. The results show that the position of the maximum LOS displacement with respect to the trench is essentially controlled by the depth of the updip slip limit (Fig. 4). As in our case InSAR measurements correspond mainly to the vertical motion, it is consistent with results from Savage (1983) showing that when the depth of the slip distribution decreases, the position of the uplift peak moves toward the trench. When the width of the slipping area increases, the position of the uplift peak remains stable, but the distance between positions of the maximum and minimum of the displacement increases (Fig. S6). Finally, increasing the amount of slip does not change the peak position as the model equations are linear. The forward model that best fits the InSAR data shows that east of the Guerrero gap, the distance between the trench and the uplift peak is greater than predicted by the slip distribution model (Radiguet et al., 2011) based only on the inversion of GPS data (Fig. 4). In agreement with our parameter analysis, the additional constraints obtained from InSAR data tend to locate the slip updip limit further downdip on the subduction interface, under the InSAR track location than the inversion entirely based on GPS data. The SSE

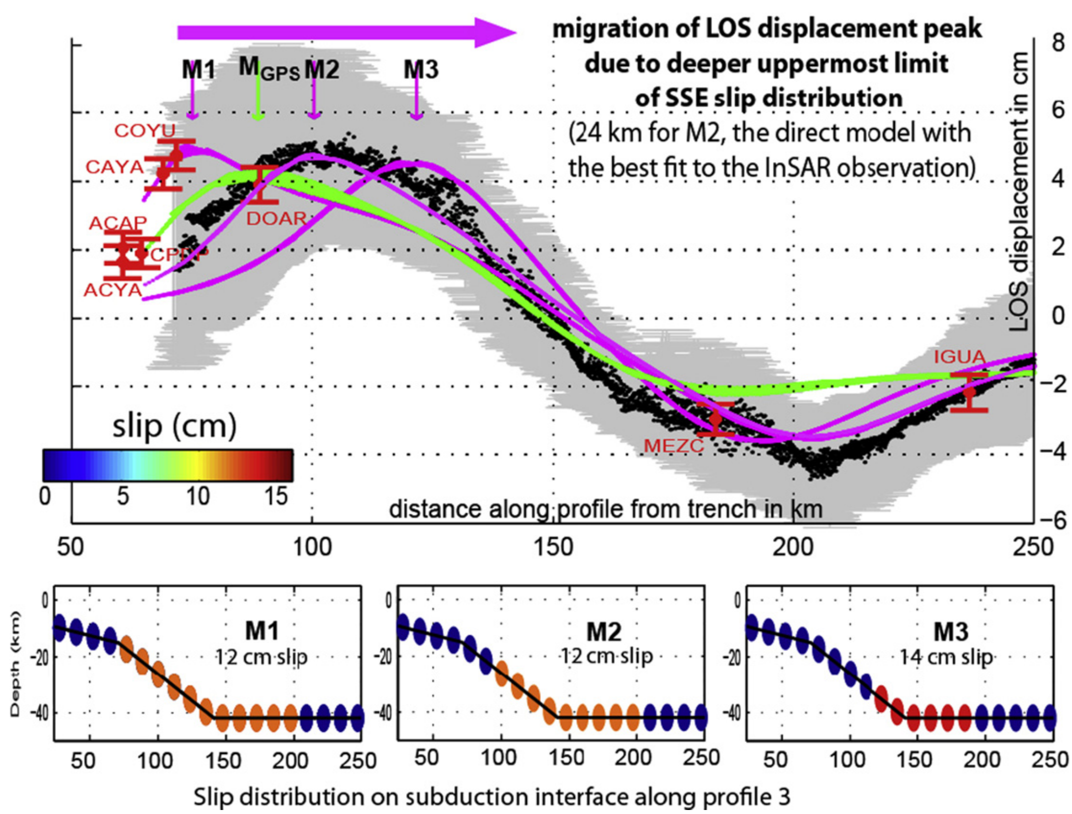


**Fig. 4.** SSE LOS displacements observed from InSAR (black dots) along the profile 3 (see location in Fig. 3) and predicted by three forward models (M1, M2 and M3). The slip distributions for the models are shown below (the color scale indicates the slip amplitude along the subfaults). The three models, with uniform slip, are the best models for an updip slip limit fixed at 15, 24, and 33 km, respectively. M2 is the best models among all the models explored (see details in text). These models have been chosen to illustrate how slip updip limit constrains the LOS displacements peak on the surface. For the best fitting model, M2, the updip limit is at 22 km depth. The comparison of InSAR displacement along profile 3 with the LOS displacement predicted by the Radiguet et al. (2011) model, green line, shows that models, constrained only by GPS data, estimate shallower updip limit of the SSE slip. This is due to the poor sampling of the displacement maximum by the sparse GPS network. The GPS inversion includes also CAYA and COYU GPS stations, located west of the profile 3, which fit better models with shallower slip (like M1). (For interpretation of the references to color in this figure legend, the reader is referred to the web version of this article.)

updip limit estimated from GPS data inversion (Radiguet et al., 2011) is between 15 and 22 km, which is shallower than the 24–28.5 km limit of the forward model that best fits the InSAR data. The difference in the estimated updip slip limits between the two models (GPS and InSAR) can be explained by the poor sampling of the uplift maximum by the GPS network due to the absence of stations between DOAR and MEZC. Moreover, in the Guerrero gap, the uniform forward models based on InSAR profiles cannot explain satisfactorily the displacements of CAYA and COYU stations at the coast. These two stations show a significantly larger horizontal and vertical SSE displacements compared to those at ACYA and ACAP (Vergnolle et al., 2010) in spite of the short distance (27 km) between COYU and ACYA. This suggests a sharp lateral variation of the slow slip distribution. To further investigate this lateral evolution of the slip distribution and its possible link with the seismic gap, we perform a joint inversion of InSAR and GPS data.

## 5. Joint inversion of InSAR and GPS data

To perform the static inversion of the GPS and InSAR cumulative displacements of the 2006 SSE, we used the method and parameterization described by Radiguet et al. (2011). It follows the formulation of Tarantola (2005) for linear problems. The cost function consist in two terms: the first term is the fit to the data, in which the data covariance matrix contains the uncertainties associated to each data, and the respective weight of InSAR and GPS data sets. The second term of the cost function is the proximity to the initial model (zero slip model). It contains the model covariance matrix used to introduce the correlation between nearby parameters. This corresponds to the addition of a smoothing operator on the slip distribution model. The correlation length (degree of smoothing) is 50 km. It was selected as the best compromise between the slip roughness and a low misfit to the data (Radiguet et al., 2012). To reduce the number of InSAR data while keeping high resolution at places where the deformation gradient is strong, we resampled the InSAR stack from $\sim 1.5 \times 10^6$ pixels to 257 pixels using a quadtree algorithm (Jónsson et al., 2002) (Fig. S7). The weight of each point is a function of the number of original pixels it contains and its standard deviation is the mean standard deviation of those pixels. One difficulty of joint inversion is to properly weight the different data sets. The relative importance between the GPS and InSAR data is introduced by a weighting factor in the data covariance matrix. Different weighting factors $w$ have been tested, where $w = w_{InSAR}/w_{GPS}$ is the ratio of the InSAR weight over the GPS weight. We then evaluate what ratio is able to explain both data sets. The agreement between data and models is defined by RMS. Fig. 5 shows the RMS between the data and the model for GPS and InSAR separately, for $w$ ranging from $10^{-3}$ to $10^3$. We see that the values of $w$ that keep a good agreement between the data and the model for both data sets lie between 1 and 5. We first inverted the data set separately to see the influence of each data type. We set $w = 1000$ and then $w = 0.001$, which almost correspond to the inversion of InSAR data or GPS data alone, respectively (Fig. 6). Then, according to the previous weighting tests (Fig. 5), we performed the joint inversion for three $w$ ratios (2, 3, and 5). Fig. 7 shows the

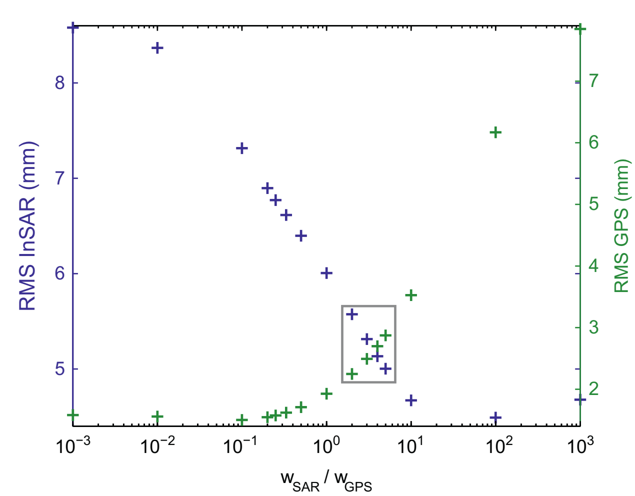


**Fig. 5.** Individual RMS values for InSAR data (blue) and GPS data (green) as a function of $w$. The gray area corresponds to the optimal $w$ values used for the inversion results shown in Figs. 7 and S6. Note that the two vertical axis have different scalings. For $w=3$, InSAR RMS are larger than GPS RMS because the standard deviations of InSAR data are larger than the standard deviations of GPS data. (For interpretation of the references to color in this figure legend, the reader is referred to the web version of this article.)

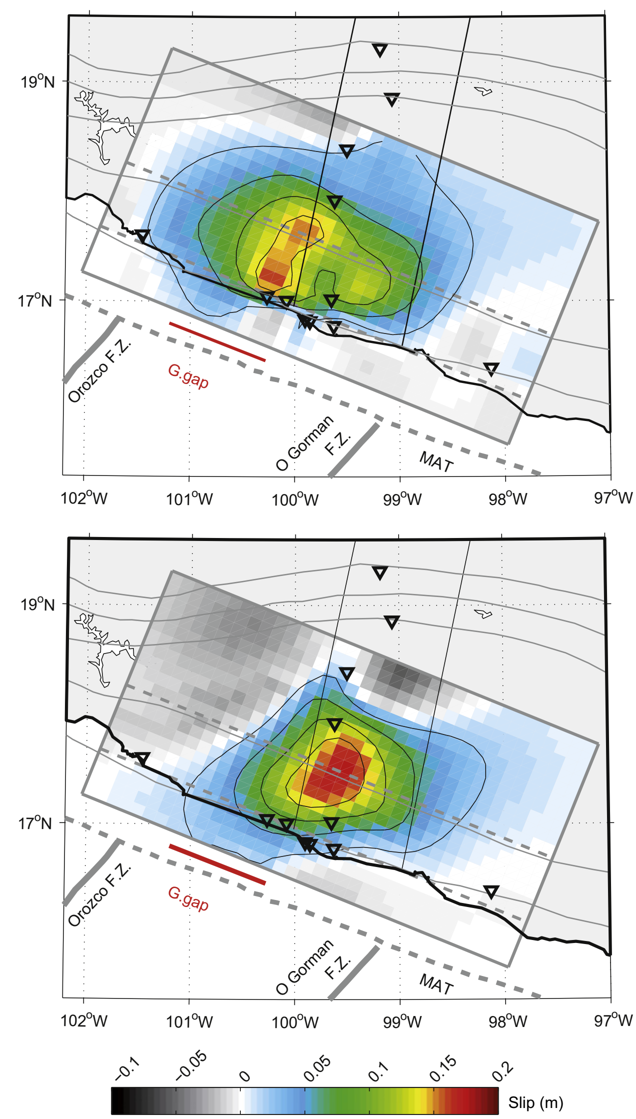


**Fig. 6.** Slip amplitude inferred by inversion with (a) $w=0.001$ (i.e. fit mainly the GPS data) or with (b) $w=1000$ (i.e. fit mainly InSAR data). GPS stations are represented by open black triangles and InSAR track by black box. Dashed thin gray lines indicate the changes in the dip of the model subduction plane (at 15 and 42 km). Dashed thick gray line represents the Middle American Trench (MAT) and thick continuous gray lines correspond to fracture zones. The location of the Guerrero gap (G.Gap) is shown in red. Negative slip values can appear because no positivity constraint is applied. They reflect uncertainties associated with the inversions. Low values of negative slip are an indication of the good quality of the model. (For interpretation of the references to color in this figure legend, the reader is referred to the web version of this article.)

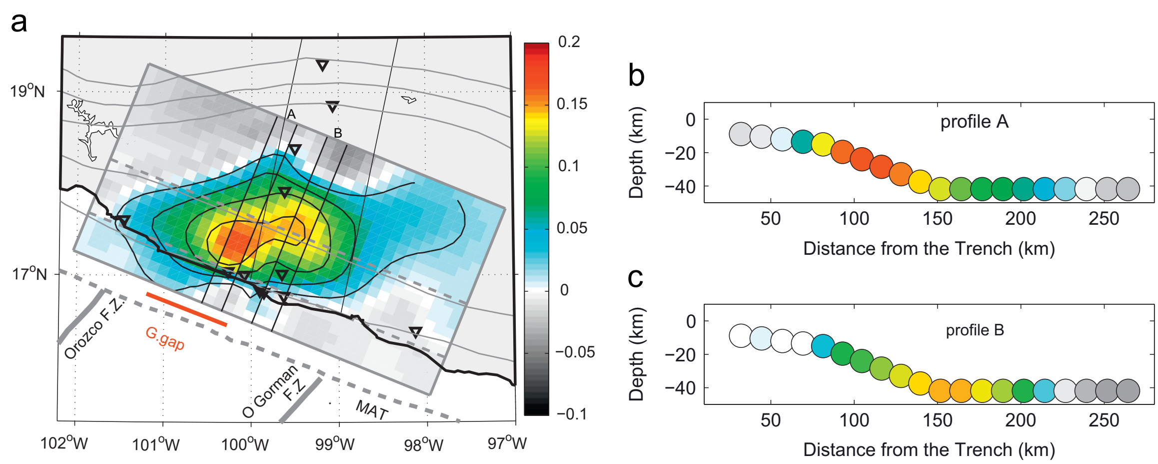


**Fig. 7.** Inversion results for $w=3$. (a) Slip distribution (in m, see the color bar) on the subduction plane. GPS stations are represented by open black triangles and InSAR track by black box. Dashed thin gray lines indicate the changes in the dip of the model subduction plane. Dashed thick gray line represents the Middle American Trench (MAT) and thick continuous gray lines correspond to fracture zones. The location of the Guerrero gap (G.Gap) is shown in red. (b) and (c) are the two profiles of this distribution across the subduction plane at locations indicated on (a). (For interpretation of the references to color in this figure legend, the reader is referred to the web version of this article.)

inversion for a ratio equal to 3. Results for a ratio of 2 and 5 give similar results (Fig. S8). Fig. 6 shows clearly that the inversion of one data type locates the slip where it can be resolved, i.e. by the observation spots. This is consistent with the resolution analysis of the inversion according to the type of data used (Radiguet et al., 2011 and Fig. S9). GPS inversion finds a shallow slip distribution with a maximum around CAYA and COYU stations while InSAR localizes most of the displacement under the track coverage with a maximum of slip at around 40 km depth. We see that the GPS inversion fits the GPS data very well, but does not reproduce precisely the LOS peak displacement observed by InSAR (Fig. 8a and d). The modelled displacement maximum is shifted toward the coast. This can be explained by the lack of GPS data needed to constrain the updip slip limit on the subduction plane as shown by the forward models analysis InSAR inversion reproduces the InSAR observations and fits relatively well the horizontal and vertical components of GPS data (Fig. 8b and d). For some stations, however, the amplitude and azimuth of modelled displacements are slightly off (e.g., COYU or CAYA stations). Note that, as previously observed with the forward approach, InSAR locates the slip deeper than the GPS along the InSAR track (i.e. east of the Guerrero gap). Inverting jointly both data sets allows one to increase the inversion resolution (Fig. S9) and thus to refine the results. Contrary to inversions with a single type of data, Fig. 7 shows a transition in the slip distribution, from a shallower patch in the seismic gap near CAYA and COYU stations ( ~ 100.2°W), to a deeper patch of slip further east ( ~ 99.5°W), in an area considered out of the Guerrero gap. According to the profiles, the maximum slip of the patch located in the gap occurs around 25 km depth (Fig. 7b), while the maximum slip on the second patch, occurs at the beginning of the flat section of the slab at 40 km depth (Fig. 7c). The continuity between the two patches is quite sensitive to the weighting parameter and the deeper slip patch is more pronounced when the relative weight of InSAR increases (Fig. S8). Fig. 8c and d shows that the joint inversion matches very well both InSAR and GPS data (global RMS=6.4 mm). As several subduction geometries have been proposed, we also checked that the results shown here do not change significantly using another subduction geometry for the inversion (e.g., Radiguet et al., 2012).

## 6. Discussion and conclusions

Combining GPS and InSAR data improves our knowledge of the slip distribution along the subduction plate interface during the 2006 SSE, especially in the eastern part of the Guerrero gap where the observation density is optimal (Fig. S9). At this location, the joint inversion reveals a lateral variation of the slip distribution along the trench that is, interestingly, spatially correlated to the eastern limit of the seismic gap delimited by the 1962 Acapulco earthquake rupture area (Ortiz et al., 2000). This observation suggests a link between the depth of the aseismic slip during the slow slip events, which repeat approximately every four years, and the recurrence interval of large earthquakes in the Guerrero subduction zone. In the seismic gap, a significant part of the aseismic slip takes place in the seismogenic zone, whereas further east, the inversion shows that the maximum of slow slip is located on the flat segment of the subduction interface (at about 40 km depth), deeper than the downdip limit of the seismogenic zone, which is expected to be at about 25 km in this section of the subduction zone (Suárez et al., 1990; Larson et al., 2004). This could explain why this area experiences more often large earthquakes like the $M_w$=7.8 event in 1957 (Ortiz et al., 2000) (Fig. 1). If the SSEs are definitively not strictly limited to the gap, the slip in it is located at a shallower depth, thus releasing in the gap part of the interseismic elastic stress that builds up in the seismogenic zone. As a consequence, it could explain the longer repeat time of large thrust earthquakes in the Guerrero Gap than in the rest of the Mexican subduction zone. Actually, no major earthquake occurred in the gap since the 1911 event, while the recurrence period out of the gap (including the segment where deeper slow slip occurs east of the gap) is estimated to be around 30–60 yrs. By improving the slip resolution, the joint inversion results support the analysis of Radiguet et al. (2012) where the slip deficit in Guerrero has been estimated over a 12 yr period (3 SSE cycles). They conclude that in the Guerrero seismic gap, the slip deficit is on average only one-quarter of what is observed on both sides of the gap. It is noteworthy that the location of this lateral transition observed at the eastern edge of the gap also corresponds to the limit of two distinct patches, in time and space, that slipped during the 2009–2010 event (Walpersdorf et al., 2011). Such a lateral variation could be controlled by heterogeneities of pore fluid pressure at the subduction interface as proposed by Song et al. (2009). For a better investigation of these phenomena, several GPS stations have been already installed after the 2006 event to increase the model resolution in the area of maximum slip in the Guerrero gap. However, as the region affected by SSEs is vast and in some places difficult to instrument, systematic InSAR coverage is still needed to complete the surface displacement observations. The Sentinel-1 C-band mission from the European Space Agency and ALOS-2 L-band mission from the Japanese Space Agency should fulfill

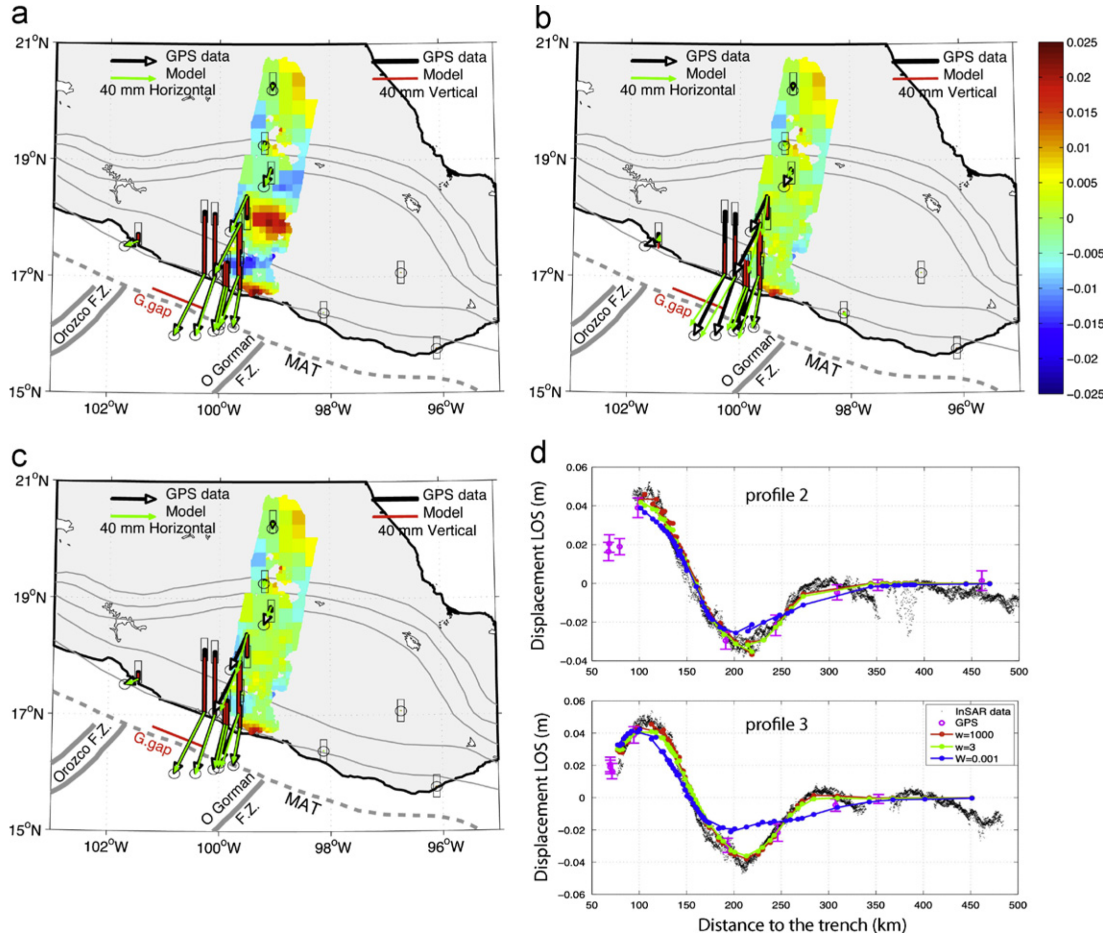


**Fig. 8.** Comparison between observed and modelled SSE displacements for inversions with $w$ equal to 0.001 (a), 1000 (b), and 3 (c). Horizontal and vertical displacements measured by GPS are the black arrows and black bars, respectively, and the modelled displacement are represented by green arrows (horizontal) and red bars (vertical). Colors correspond to the residues (in meter, see the color scale) between LOS InSAR displacement and LOS modelled displacement. (d) Comparison between the observed and the modelled displacement along the profiles 2 and 3 shown in Fig. 3. GPS data are projected to the LOS (purple dots), InSAR measurements are the black dots. The blue, green, and red curves correspond to LOS modelled displacements with $w$ equal to 0.001, 3, and 1000, respectively. (For interpretation of the references to color in this figure legend, the reader is referred to the web version of this article.)

this requirement (both satellites are planned to be launched in 2013). These new data sets will be decisive to observe in details the whole Guerrero gap, and in particular to establish possible similar behaviors in the western side of the Guerrero gap where currently very few geodetic data exists.

## Acknowledgments

This work has been supported by the French national research agency through the project ANR-G-GAP RA0000C069 and by INSU project PNTS AO2006 and a CNRS postdoctoral fellowship. We would like to thank the European Space Agency (ESA) for providing Envisat images through category 1 project #5036. GPS network maintenance and data acquisition were funded by COANCYT 46064, 84544 and PAPIIT IN103808, and IN 114611 grants. We thank the two anonymous reviewers for their helpful comments.

## Appendix A. Supplementary material

Supplementary data associated with this article can be found in the online version at http://dx.doi.org.10.1016/j.epsl.2013.02.020.

## References

Bürgmann, R., Rosen, P.A., Fielding, E.J., 2000. Synthetic Aperture Radar interferometry to measure Earth's surface topography and its deformation. Annu. Rev. Earth. Planet. Sci. 28, 169–209.

Cavalié, O., Doin, M.-P., Lasserre, C., Briole, P., 2007. Ground motion measurement in the Lake Mead area, Nevada, by differential synthetic aperture radar interferometry time series analysis: probing the lithosphere rheological structure. J. Geophys. Res. 112 (B3).

Cavalié, O., Lasserre, C., Doin, M.-P., Peltzer, G., Sun, J., Xu, X., Shen, Z.-K., 2008. Measurement of interseismic strain across the Haiyuan fault (Gansu, China), by InSAR. Earth. Planet. Sci. Lett. 275, 246–257.

Cavalié, O., Pathier, E., Cotton, F., Doin, M.-P., Cotte, N., Vergnolle, M., Walpersdorf, A., 2009. Mapping of the 2006 silent slow event in the Guerrero (Mexico) seismic gap by InSAR. EGU General Assembly 11, EGU2009-5133.

Chen, C.W., Zebker, H.A., 2000. Network approaches to two-dimensional phase unwrapping: intractability and two algorithms. J. Opt. Soc. Am. A 17 (3).

Demets, C.R., Gordon, R., Argus, D., 2010. Geologically current plate motions. Geophys. J. Int. 181, 1–80.

Doin, M.-P., Lasserre, C., Peltzer, G., Cavalié, O., Doubre, C., 2009. Corrections of stratified tropospheric delays in SAR interferometry: validation with global atmospheric models. J. Appl. Geophys. 101 (B7), 16119–16135.

Dragert, H., Wang, K., Rogers, G., 2004. Geodetic and seismic signatures of episodic tremor and slip in the northern Cascadia subduction zone. Geology 56, 1143–1150.

Farr, T.G., Kobrick, M., 2000. Shuttle radar topography mission produces a wealth of data. Eos Trans. AGU 81 (48), 583–585.

Ferretti, A., Monti-Guarnieri, A., Prati, C., Rocca, C., Massonnet, D., 2007. InSAR Principles: Guidelines for SAR Interferometry Processing and Interpretation. ESA Publications.

Gens, R., 2003. Two-dimensional phase unwrapping for radar interferometry: developments and new challenges. Int. J. Remote Sensing 24 (4), 703–710.

Goldstein, R.M., Werner, C.L., 1998. Radar interferogram filtering for geophysical applications. Geophys. Res. Lett. 25 (21), 2517–2520.
Hanssen, R.F., 2001. Radar Interferometry, Data Interpretation and Error Analysis. Kluwer Academic Publishers.
Hernandez, B., Shapiro, N.M., Singh, S.K., Pacheco, J.F., Cotton, F., Campillo, M., Iglesias, A., Cruz, V., Gomez, J.M., Alcantara, L., 2001. Rupture history of September 30, 1999 intraplate earthquake of Oaxaca, Mexico ($M_w$=7.5) from inversion of strong-motion data. Geophys. Res. Lett. 385 (28), 363–366.
Hirose, H., Obara, K., 2005. Repeating short- and long-term slow slip events with deep tremor activity, around the Bungo channel region, southwest Japan. Earth Planets Space 57, 961–972.
Hooper, A., Bekaert, D., Spaans, K., Arikan, M., 2012. Recent advances in SAR interferometry time series analysis for measuring crustal deformation. Tectonophysics 513–517, 1–13.
Hooper, A., Zebker, H., Segall, P., Kampes, B., 2004. A new method for measuring deformation on volcanoes and other natural terrains using InSAR persistent scatterers. Geophys. Res. Lett. 31.
Ide, S., Beroza, G.C., Shelly, D.R., Uchide, T., 2007. A scaling law for slow earthquakes. Nature 447, 76–79.
Jónsson, S., 2008. Importance of post-seismic viscous relaxation in southern Iceland. Nat. Geosci. 1, 136–139.
Jónsson, S., Zebker, H., Segall, P., Amelung, F., 2002. Fault slip distribution of the 1999 $M_W$ 7.1 Hector Mine, California, earthquake, estimated from satellite radar and GPS measurements. Bull. Seismol. Soc. Am. 92 (4), 1377–1389.
Kerr, R.A., 2011. New work reinforces megaquake's harsh lessons in geoscience. Science 332 (6032).
Kostoglodov, V., Husker, A., Shapiro, N.M., Payero, J.S., Campillo, M., Cotte, N., Clayton, R., 2010. The 2006 slow slip event and nonvolcanic tremor in the Mexican subduction zone. Geophys. Res. Lett. 37 (L24301).
Kostoglodov, V., Ponce, L., 1994. Relationship between subduction and seismicity in the Mexican part of the Middle America trench. J. Geophys. Res. 99, 729–742.
Kostoglodov, V., Singh, S.K., Santiago, J.A., Franco, S.I., Larson, K.M., Lowry, A.R., Bilham, R., 2003. A large silent earthquake in the Guerrero seismic gap, Mexico. Geophys. Res. Lett. 30.
Larson, K.M., Kostoglodov, V., Miyazaki, S., Santiago, J.-A., 2007. The 2006 aseismic slow slip event in Guerrero, Mexico: new results from GPS. Geophys. Res. Lett. 34 (L13309).
Larson, K.M., Lowry, A.R., Kostoglodov, V., Hutton, W., Sánchez, O., Hudnut, K., Suárez, G., 2004. Crustal deformation measurements in Guerrero, Mexico. J. Geophys. Res. 109 (B04409).
López-Quiroz, P., Doin, M.-P., Tupin, F., Briole, P., Nicolas, J.-M., 2009. Time series analysis of Mexico City subsidence constrained by radar interferometry J. Appl. Geophys. 69 (1).
Loveless, J., Meade, B.J., 2010. Geodetic imaging of plate motions, slip rates, and partitioning of deformation in Japan. J. Geophys. Res. 115 (B02410).
Lowry, A.R., Larson, K.M., Kostoglodov, V., Bilham, R., 2001. Transient fault slip in Guerrero, southern Mexico. Geophys. Res. Lett. 28 (19), 3753–3756.
Mazzotti, S., Adams, J., 2004. Variability of near-term probability for the next great earthquake on the Cascadia subduction zone. Bull. Seismol. Soc. Am. 94 (5), 1954–1959.
Nishenko, S.P., Singh, S.K., 1987. Conditional probabilities for the recurrence of large and great interplate earthquakes along the Mexican subduction zone. Bull. Seismol. Soc. Am. 77 (6).
Ortiz, M., Singh, S.K., Kostoglodov, V., Pacheco, J., 2000. Constraint on the rupture areas of the Acapulco San Marcos, Mexico earthquakes of the 1962 ($M$7.1, 7.0) and 1957 ($M$7.7), based on the analysis of tide records. Geofis. Int. 39, 337–348.
Payero, J.S., Kostoglodov, V., Shapiro, N., Mikumo, T., Iglesias, A., Perez-Campos, X., Clayton, R.W., 2008. Nonvolcanic tremor observed in the Mexican subduction zone. Geophys. Res. Lett. 35 (L07305).
Radiguet, M., Cotton, F., Vergnolle, M., Campillo, M., Valette, B., Kostoglodov, V., Cotte, N., 2011. Spatial and temporal evolution of a long term slow slip event: the 2006 Guerrero Slow Slip Event. Geophys. J. Int. 184 (2), 816–828.
Radiguet, M., Cotton, F., Vergnolle, M., Campillo, M., Walpersdorf, A., Cotte, N., Kostoglodov, V., 2012. Slow slip events and strain accumulation in the Guerrero gap, Mexico. J. Geophys. Res. 117 (B04305).
Rosen, P.A., Hensley, S., Peltzer, G., Simons, M., 2004. Updated repeat orbit interferometry package released. Eos Trans. AGU 85 (5), 47.
Savage, J.C., 1983. A dislocation model of strain accumulation and release at a subduction zone. J. Geophys. Res. 88, 4984–4996.
Scharroo, R., Visser, P.N.A.M., 1998. Precise orbit determination and gravity field improvement for the ERS satellites. J. Geophys. Res. 103 (C4), 8113–8127.
Song, T.-R.A., Helmberger, D.V., Brudzinski, M.R., Clayton, R.W., Davis, P., Perez-Campos, X., Singh, S.K., 2009. Subducting slab ultra-slow velocity layer coincident with silent earthquakes in southern Mexico. Science 324 (5926), 502–506.
Suárez, G., Monfret, T., Wittlinger, G., David, C., 1990. Geometry of subduction and depth of the seismogenic zone in the Guerero gap, Mexico. Nature 345, 336–338.
Tarantola, A., 2005. Inverse Problem Theory and Methods for Model Parameter Estimation. Society for Industrial and Applied Mathematics (SIAM), Philadelphia.
Vergnolle, M., Walpersdorf, A., Kostoglodov, V., Tregoning, P., Santiago, J.A., Cotte, N., Franco, S.I., 2010. Slow slip events in Mexico revised from the processing of 11 year GPS observations. J. Geophys. Res. 115 (B08403).
Walpersdorf, A., Cotte, N., Kostoglodov, V., Vergnolle, M., Radiguet, M., Santiago, J.S., Campillo, M., 2011. Two successive slow slip events evidenced in 2009–2010 by a dense GPS network in Guerrero, Mexico. Geophys. Res. Lett. 38 (L15307).
Yoshioka, S., Mikumo, T., V. Kostoglodov, K.M.L., Lowry, A.R., Singh, S.K., 2004. Interplate coupling and a recent aseismic slow slip event in the Guerrero seismic gap of the Mexican subduction zone, as deduced from GPS data inversion using a Bayesian information criterion. Phys. Earth Planet. Int. 146, 513–530.
Zebker, H.A., Rosen, P.A., Hensley, S., 1997. Atmospheric effects in interferometric synthetic aperture radar surface deformation and topographic maps. J. Geophys. Res. 102 (B4), 7547–7563.